Available online at www.sciencedirect.com
ScienceDirect
Biochimica et Biophysica Acta 1778 (2008) 491–501
Biochimica et Biophysica Acta
BBA
www.elsevier.com/locate/bbamem

Effects of fluorescent probe NBD-PC on the structure, dynamics and phase transition of DPPC. A molecular dynamics and differential scanning calorimetry study

Luís M.S. Loura [a,b,*], Fábio Fernandes [c], A.C. Fernandes [d], J.P. Prates Ramalho [b,e]

[a] *Faculdade de Farmácia, Universidade de Coimbra, Rua do Norte, 3000-295 Coimbra, Portugal*
[b] *Centro de Química de Évora, Universidade de Évora, Rua Romão Ramalho, 59, 7000-671 Évora, Portugal*
[c] *Centro de Química-Física Molecular, Complexo I, Instituto Superior Técnico, Av. Rovisco Pais, 1049-001 Lisboa, Portugal*
[d] *Centro de Química Estrutural, Complexo I, Instituto Superior Técnico, Av. Rovisco Pais, 1049-001 Lisboa, Portugal*
[e] *Departamento de Química, Universidade de Évora, Rua Romão Ramalho, 59, 7000-671 Évora, Portugal*

Received 14 June 2007; received in revised form 16 October 2007; accepted 24 October 2007
Available online 1 November 2007

Abstract

We present a combined theoretical (molecular dynamics, MD) and experimental (differential scanning calorimetry, DSC) study of the effect of 7-nitrobenz-2-oxa-1,3-diazol-4-yl (NBD) acyl chain-labeled fluorescent phospholipid analogs (C6-NBD-PC and C12-NBD-PC) on 1,2-dipalmitoyl-*sn*-glycero-3-phosphocholine (DPPC) bilayers. DSC measurements reveal that <1 mol% of NBD-PC causes elimination of the pre-transition and a large loss of cooperativity of the main transition of DPPC. Labeling with C6-NBD-PC or C12-NBD-PC shifts the main transition temperature to lower or higher values, respectively. Following our recent report on the location and dynamics of these probes (*BBA* 1768 (2007) 467–478) in fluid phase DPPC, we present a detailed analysis of 100-ns MD simulations of systems containing either C6-NBD-PC or C12-NBD-PC, focused on their influence on several properties of the host bilayer. Whereas most monitored parameters are not severely affected for 1.6 mol% of probe, for the higher concentration studied (6.2 mol%) important differences are evident. In agreement with published reports, we observed that the average area per phospholipid molecule increases, whereas DPPC acyl chain order parameters decrease. Moreover, we predict that incorporation of NBD-PC should increase the electrostatic potential across the bilayer and, especially for C12-NBD-PC, slow lateral diffusion of DPPC molecules and rotational mobility of DPPC acyl chains.

Keywords: Fluorescence probe; NBD-labeled lipid; Molecular simulation; Membrane model system; Membrane perturbation

1. Introduction

Fluorescence spectroscopy and microscopy have been widely used in the last decades as powerful approaches for studying organization and dynamics in membranes (see e.g. [1,2] for recent reviews). The advantages of fluorescence include high sensitivity and time resolution, multiple measurable parameters yielding complementary information, and, in the case of fluorescence microscopy, spatial resolution. However, fluorescence studies of membranes require the use of fluorescent probes, which can potentially cause significant perturbation to membrane structure, dynamics and thermotropic behavior, as long reported in literature experimental works (e.g. [3–6]). Therefore, when interpreting the results of fluorescence experiments, it can be hard to distinguish between legitimate membrane properties and perturbing effects resulting from probe incorporation.

To this effect, molecular dynamics (MD) simulations, by providing detailed atomic-scale information on phospholipid bilayers [7,8], represent a valuable way to detect and quantify the magnitude of perturbation induced by molecular probes on the host lipid structure. Area per lipid, mass distributions, order parameters, diffusion coefficients and interface and electrostatic properties can be determined and compared in the absence and

* Corresponding author. Faculdade de Farmácia, Universidade de Coimbra, Rua do Norte, 3000-295 Coimbra, Portugal.
E-mail address: lloura@ff.uc.pt (L.M.S. Loura).

0005-2736/$ - see front matter © 2007 Elsevier B.V. All rights reserved.
doi:10.1016/j.bbamem.2007.10.022

presence of a given probe, enabling a good judgement of whether the latter is adequate as a reporter of lipid bilayer structure and dynamics. Surprisingly, detailed MD studies of probe influence on membranes are scarce and mostly restricted to recent works using apolar fluorophores such as diphenylhexatriene (DPH; [9]), free pyrene [10] or pyrene-labeled phosphatidylcholine [11]. To our knowledge, no studies have been published with probes made up of phospholipids labeled with a polar fluorophore group. These constitute a very important class of membrane probes, as increasingly more head- and acyl chain-labeled phospholipids derivatives become commercially available. Among the latter, a popular family is that of phospholipids labeled with the 7-nitrobenz-2-oxa-1,3-diazol-4-yl (NBD) fluorophore in one of the acyl chains (see [12] for a review). NBD derivatives are commercially available for all major phospholipid classes, and have been used extensively as fluorescent analogs of native lipids in biological and model membranes to study a variety of processes [12–14]. As a fluorophore, NBD possesses convenient photophysical properties, such as good fluorescence quantum yield, environment sensitivity, and suitability for fluorescence resonance energy transfer experiments, as a donor (namely to rhodamine-based probes e.g., [15,16]) or acceptor, e.g., to DPH probes [17], and in homotransfer studies of lipid aggregation.

However, as verified experimentally by several authors [13,18–20], and in accordance with our own MD simulations [21], the NBD group of *sn*-2 acyl chain NBD-labeled phosphatidylcholine (NBD-PC) is prone to loop to a location near the lipid/water interface. From our simulations, the most probable transverse location of the NBD moiety of NBD-PC in fluid DPPC bilayers is the glycerol backbone/carbonyl region. This results in a u-turn-like arrangement for the labeled *sn*-2 chain of C12-NBD-PC (see Fig. 1 for structure), the 9th C atom of the *sn*-2 chain being the one closest to the bilayer center. On the other hand, the shorter labeled *sn*-2 chain of C6-NBD-PC (see Fig. 1 for structure) does not penetrate the bilayer beyond the C4–C5 atoms of *sn*-2 chains of the host lipid, and lies in an extended conformation, almost parallel to the bilayer plane. Based on these observations, it is plausible that incorporation of NBD-PC probes will cause significant perturbation to the host bilayer structure. This work combines MD simulations and differential scanning

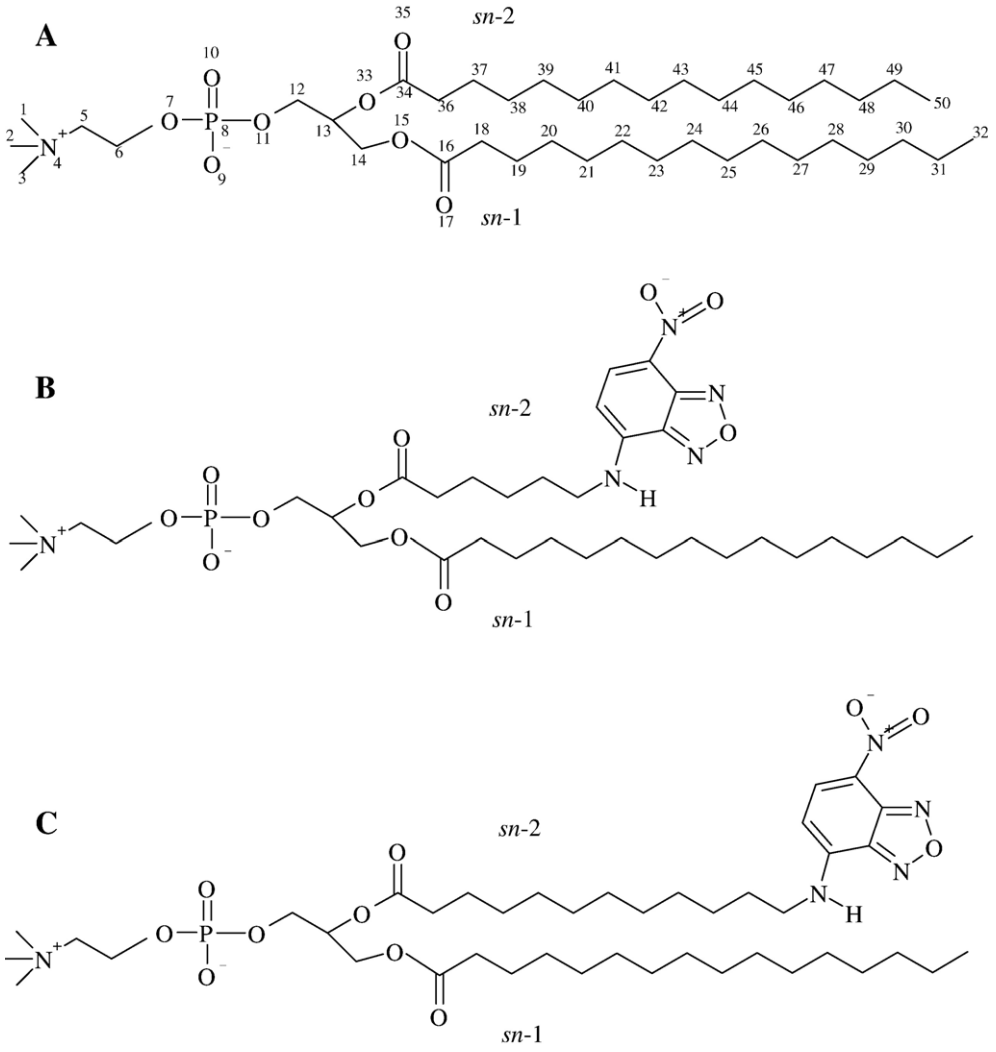

Fig. 1. Structures of (A) DPPC, (B) C6-NBD-PC and (C) C12-NBD-PC, showing the atom numbering of DPPC as used in the text.

calorimetry (DSC) measurements to address this issue. It is concluded that whereas important effects are indeed observed for high (~6 mol%) probe content, milder perturbation of fluid DPPC structure and dynamics is expected for ~1 mol% or less probe, the concentrations most often used experimentally. However, even for these smaller amounts, large alterations (transition temperature shifts, loss of cooperativity), are evident in the thermotropic behavior of NBD-PC labeled DPPC bilayers, hampering the use of these fluorescent probes in the context of the study of phospholipid phase transitions.

2. Materials and methods

2.1. Materials

1,2-dipalmitoyl-*sn*-glycero-3-phosphocholine (DPPC, Fig. 1A), 1-palmitoyl-2-[6-(7-nitrobenz-2-oxa-1,3-diazol-4-yl)aminododecanoyl]-*sn*-glycero-3-phosphocholine (C6-NBD-PC, Fig. 1B) and 1-palmitoyl-2-[12-(7-nitrobenz-2-oxa-1,3-diazol-4-yl)aminododecanoyl]-*sn*-glycero-3-phosphocholine (C12-NBD-PC, Fig. 1C) were obtained from Avanti Polar Lipids (Birmingham, AL). 4-(2-hydroxyethyl)-1-piperazine sulfonic acid (HEPES), KOH and KCl (all from Merck, Darmstadt, Germany) were used to prepare the buffer solution 20 mM HEPES-KOH (pH 7.4). All organic solvents were of spectroscopic grade and came from Merck (Darmstadt, Germany). Deionized water was used throughout. All above materials were used without further purification. The concentrations of stock solutions of the probes were determined spectrophotometrically using ε (NBD-PC, 465 nm, in C_2H_5OH)=2.2×10^4 M^{-1} cm^{-1} [22].

2.2. Lipid vesicle preparation

Samples were hydrated in 20 mM HEPES buffer (pH 6.8) at 65 °C and submitted to 8 freeze–thaw-vortex cycles between liquid nitrogen temperature and a water bath at 65 °C. The final concentration of DPPC+NBD-PC in the solutions was 0.5 mM. The concentrations of phospholipid stock solutions were determined using phosphate analysis [23]. The resulting lipid dispersions were stored at room temperature and used within 24 h of preparation.

2.3. Differential scanning calorimetry

Differential scanning calorimetry (DSC) measurements were performed in a VP-DSC Microcal (Northampton, MA) differential scanning calorimeter. Before being loaded into the DSC, samples were incubated at 65 °C for 1 h and degassed under vacuum. Heating scans were run with a rate of 1 °C/min. Thermogram decomposition, transition temperatures, enthalpies, and widths at half-height were determined using the software ORIGIN (MicroCal) provided with the calorimeter. This software uses the Levenberg/Marquardt nonlinear least-squares method for curve fitting. A model assuming independent non-two-state transitions provided the best fit to the experimental data [24]. Cooperative unit values were calculated as the ratio of van't Hoff and calorimetric enthalpies recovered from the model fits.

2.4. MD simulations

Details regarding the MD simulations were presented elsewhere [21]. Briefly, five 100-ns run of 64 phospholipid molecules and 1947 SPC [25] water molecules were carried out. In one simulation, all phospholipid molecules were unlabeled DPPC. The starting configuration of this bilayer was downloaded from the Tieleman group web page (http://moose.bio.ucalgary.ca/files/dppc64.pdb) and stripped of the 1917 outermost water molecules, leaving still enough water content (water:lipid ratio=32) for full bilayer hydration [26]. In two other simulations, one DPPC molecule was replaced by either a C6-NBD-PC or a C12-NBD-PC molecule. In two further simulations, four DPPC molecules were replaced by either four C6-NBD-PC or four C12-NBD-PC molecules (two in each bilayer leaflet in both cases).

All calculations were carried out with Gromacs 3.2 [27,28], under constant number of particles, pressure and temperature (323 K), and with periodic boundary conditions. Pressure and temperature control was carried out using the weak-coupling Berendsen schemes [29], with coupling times of 1.0 ps and 0.1 ps, respectively. Semiisotropic pressure coupling was used. All bonds were constrained to their equilibrium values, using the SETTLE algorithm [30] for water and the LINCS algorithm [31] for all other bonds, allowing the use of a time-step of 4 fs [32,33]. The long-range electrostatics Particle Mesh Ewald treatment [34] was applied, and van der Waals interactions were cut off at 0.9 nm [9,35]. Regarding the latter parameter, the use of 0.9 nm instead of a slightly higher value (say, 1.0 nm) might lead to a minor effect in the area per molecule, which, according to Repáková et al. [9] did not significantly affect the analysis of probe properties and probe-related effects in their studies of DPH-labeled DPPC membranes [9,35]. Parameters for bonded and nonbonded interactions of the DPPC molecule were taken from [36] and are available at the GROMACS home page in http://www.gromacs.org/contributed_by_users/task,doc_download/gid,40/. This force field uses united-atom description for CH, CH_2, and CH_3 groups. The partial charge distribution for DPPC in the underlying model, taken from http://moose.bio.ucalgary.ca/files/dppc.itp, was used. For the C6-NBD-PC and C12-NBD-PC molecules, parameters were based on those of DPPC, except for the fluorophore atoms. For these, modified parameters were obtained as described in detail elsewhere [21]. Unless stated otherwise, the first 10 ns of each simulation were used for equilibration, and the remaining 90 ns were used for analysis.

The electrostatic potential across the bilayer (z coordinate) was calculated by double integration of the charge density:

$$\psi(z)-\psi(\infty)=-\frac{1}{\varepsilon_0}\int_z^{\infty}dz'\int_{z'}^{\infty}\rho(z'')dz'' \quad (1)$$

For this calculation (as well as for mass density profiles), and because the bilayers' centers of mass may fluctuate in time, the positions of all atoms were determined relative to the instantaneous center of mass (z=0) in all simulations, for each frame. The potential was also averaged and symmetrized for the two bilayer leaflets [37].

3. Results and discussion

3.1. DSC

Fig. 2 shows DSC results of pure DPPC, as well as DPPC/C6-NBD-PC (Fig. 2A) and DPPC/C12-NBD-PC (Fig. 2B), obtained on heating. The results measured for the pre-transition temperature (T_p=35.2 °C), main transition temperature (T_m=41.39±0.01 °C) and calorimetric enthalpy of the main transition (8914±62 cal/mol) of DPPC agree well with literature values [38,39]. The determined cooperative unit of 161±3 lies within the range of published values (70–260) [38–40].

Upon addition of C6-NBD-PC, major changes are apparent in the scans. Firstly, there is a decrease in the main transition temperature (see Fig. 3A), from 41.4 °C (pure DPPC) to 40.8 °C (4 mol% of C6-NBD-PC; for the sample with 6 mol% C6-NBD-PC, two peaks are required for analysis, with T_m=40.85 and T_m=43.55, respectively, and forcing a single peak leads to recovery of T_m=41.3 °C). Secondly, the transitions become significantly broader. The cooperative unit decreases from 161 to 16 as the mole fraction of C6-NBD-PC increases from 0 to 6.25% (Fig. 3B). This happens without significant changes in the transition enthalpy per mole of total phospholipid (probe included; Fig. 3C), with fluctuations around an average of ~9 kcal/mol being probably due to variations in volume and/or concentration between samples. In addition, the pre-transition vanishes even for <1 mol% of probe.

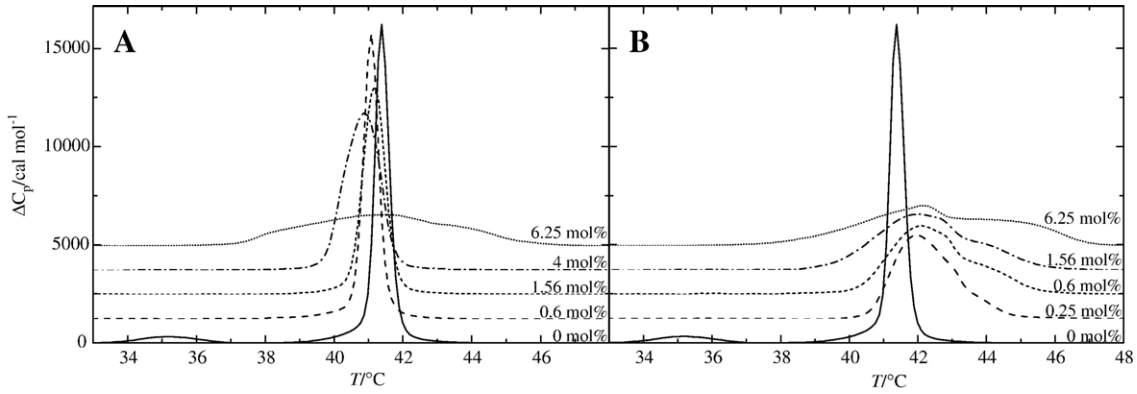

Fig. 2. DSC upscans of DPPC bilayers labeled with varying quantities of C6-NBD-PC (A) and C12-NBD-PC (B).

The effect of C12-NBD-PC on the scans differs from that of C6-NBD-PC on several aspects. Fig. 3A, B and C shows the variations of main transition temperature, cooperative unit and transition enthalpy (respectively) recovered from the single transition fits, in comparison to the values obtained in the presence of C6-NBD-PC. Similar to the latter, there is a large loss of transition cooperativity upon increasing concentration of C12-NBD-PC (the decrease of cooperative unit is even steeper than that verified for C6-NBD-PC). However, unlike the shorter chain probe, the main transition enthalpy increases steadily with increasing probe content (by almost 20% for 6.25 mol% of C12-NBD-PC) and, most significantly, the transition temperature varies in the opposite way, that is, it *increases* by more than 1 °C as C12-NBD-PC varies in the 0–6.25 mol% range. Inclusion of a second, higher temperature peak (which becomes increasingly important for higher probe content) in the analyses leads to better fitting to the data (not shown), but does not add significantly to this discussion. Briefly, the lower T_m (T_{m1}) increases to an approximately constant value 42±1 °C for >0.6 mol% of probe, whereas the higher T_m (T_{m2}; associated to the secondary peak in the scans) increases from 42.8±0.1 °C for 0.2 mol% to 45.1±0.1 °C for 6.25 mol%. In this analysis, the overall transition enthalpy is split between the two transitions, with e.g. ΔH_1=8.0±0.1 cal/mol and ΔH_2=2.1±0.1 kcal/mol being obtained for 6.25 mol%. The cooperative unit associated to the primary peak decreases, albeit less steeply than in the one-transition model (e.g., 106±14 and 23±1 are the values calculated for 0.2 and 6.25 mol%, respectively), whereas that associated to the secondary peak varies non-monotonously. The observation of two peaks in the DSC scans is probably indicative of phase separation below T_m, with formation of probe-rich and probe-poor domains, which would melt at slightly different temperatures. In any case, from the scans it can be seen that the phase transition is complete at 323 K (temperature at which the MD simulations were carried out), even for the systems with higher probe content. At this temperature, DSC is unable to reveal eventual fluid–fluid heterogeneity.

In summary, inclusion of both probes eliminates the pre-transition and broadens the main transition of DPPC. Main transition enthalpy does not vary significantly upon addition of C6-NBD-PC, and increases somewhat upon addition of C12-NBD-PC. The two probes have opposing effects upon the main transition temperature, with C6-NBD-PC leading to its decrease and C12-NBD-PC leading to its increase.

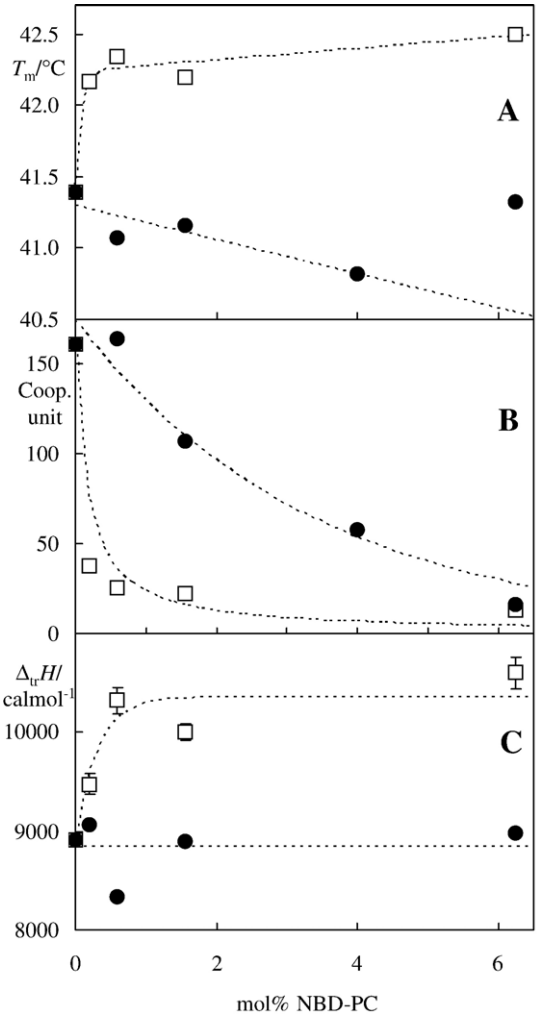

Fig. 3. Main transition temperature (T_m, A), cooperative unit (B) and transition enthalpy ($\Delta_{tr}H$, C) of labeled DPPC bilayers for varying content of C6-NBD-PC (●) and C12-NBD-PC (□). The lines are mere guides to the eye. Calculations of all parameters shown assume a single transition peak. Note that the unexpectedly high T_m obtained for the sample with 6.25 mol% of C6-NBD-PC is probably related to the fact that for this sample two peaks would actually be required for a successful analysis (see text for further details).

3.2. MD simulations

3.2.1. Area per phospholipid

Fig. 4 shows the time evolution of the area per lipid molecule a, calculated as the instant box area divided by the number of lipid molecules in each monolayer (32), for pure DPPC bilayers (A), 1:63 C6-NBD-PC/DPPC (B) and C12-NBD-PC/DPPC bilayers (C), and 4:60 C6-NBD-PC/DPPC (D) and C12-NBD-PC/DPPC bilayers (E). As discussed previously regarding the DPPC and 1:63 NBD-PC simulations [21], the initial structures are already close to equilibrium, justifying the chosen time range for analysis of [10 ns, 100 ns], and the average value of $a=0.669\pm0.004$ nm^2 for DPPC agrees with both experimental and theoretical literature values [35,37,41–43]. Whereas the values obtained for the averages of a in the 1:63 NBD-PC simulations do not differ significantly from that of DPPC ($a=0.669\pm0.004$ m^2 for 1:63 C12-NBD-PC/DPPC and 0.667 ± 0.004 nm^2 for 1:63 C6-NBD-PC/DPPC), that is no longer the case for the 4:60 NBD-PC simulations. For these systems, higher values are obtained for the average area per lipid ($a=0.680\pm0.003$ nm^2 for 4:60 C6-NBD-PC/DPPC and 0.681 ± 0.003 nm^2 for 4:60 C12-NBD-PC/DPPC). This increase is not surprising, given the "snorkeling" tendency of the *sn*-2 chain of both NBD-PC lipids (see e.g. Fig. 8 of [21]), leading to the probe molecule occupying a larger area in the interface region of the bilayer. This agrees with the NMR measurements of the deuterium order parameter in NBD-PC/POPC bilayers of Huster et al. [20], which led these authors to estimate an increase of ~0.2 nm^2 in area per POPC molecule for bilayers with 25 mol% of NBD-PC.

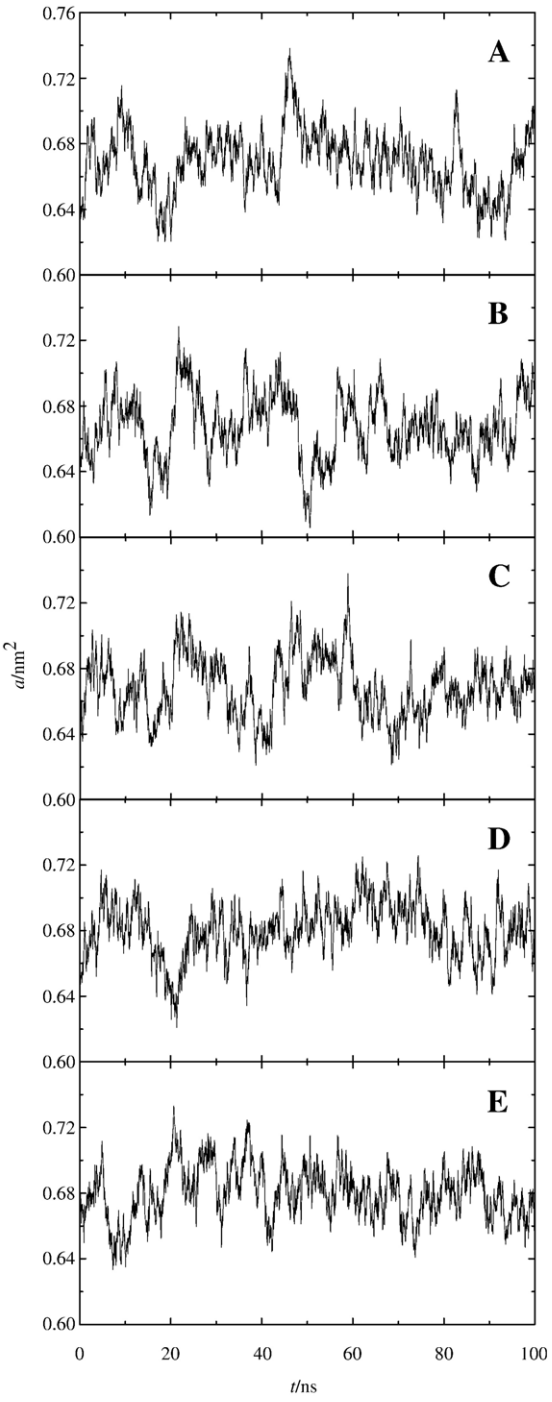

Fig. 4. Instant area/lipid molecule (a) for (A) pure DPPC, (B) 1 C6-NBD-PC:63 DPPC, (C) 1 C12-NBD-PC:63 DPPC, (D) 4 C6-NBD-PC:60 DPPC and (E) 4 C12-NBD-PC:60 DPPC.

3.2.2. Order parameters

The deuterium order parameter across the acyl chain, S_{CD}, is calculated for C atom i of the lipid acyl chains from $S_{CD,i}=-S_{zz,i}/2$, where

$$S_{zz,i}(i)=\left\langle\frac{1}{2}\left(3\cos^2\theta_{z,i}-1\right)\right\rangle \quad (2)$$

in which $\theta_{z,i}$ is the angle between the vector uniting C atoms $i-1$ and $i+1$ and the bilayer normal (z axis; [44]). $-S_{CD}$ can vary between 0.5 (full order along the bilayer normal) and −0.25 (full order along the bilayer plane), whereas $S_{CD}=0$ denotes isotropic orientation. Fig. 5A shows $-S_{CD}$ for the *sn*-1 chains' C atoms of DPPC for pure DPPC and 4 NBD-PC:60 NBD-PC bilayers. Due to the slow convergence of this parameter [45], analysis was restricted to the last 25 ns of the simulations. In general, incorporation of NBD-PC leads to a reduction in the order parameter of the DPPC acyl chain atoms (this is also verified, to a lesser extent, in the 1 NBD-PC:63 DPPC simulations (not shown)). This effect is more pronounced in the C9–C12 region (see Fig. 5B), in agreement with the NMR data of Huster et al. [20] for NBD-PC:POPC. In these authors' results, there is no clear distinction between the effects of C6-NBD-PC and C12-NBD-PC. The fact that a larger decrease in $-S_{CD}$ was obtained for C6-NBD-PC in this study is possibly not significant (for the 1 NBD-PC:63 DPPC simulations, a larger decrease is observed for C12-NBD-PC than C6-NBD-PC; not shown). In any case, it is clear that NBD-PC probes lead to a decreased order in the host DPPC acyl chains, more markedly in the C9–C12 region, in agreement with the experimental data of Huster et al. [20]. The fact that this order decrease is less marked in the C13–C15 region is probably justified by the fact that, even in the absence of probe, this bilayer region is already characterized by a high degree of orientational disorder of the lipid chains. For C16, there is reportedly almost no reduction in $-S_{CD}$ [20]. Because of the way GROMACS calculates $-S_{CD}$ for atom i of a given acyl chain

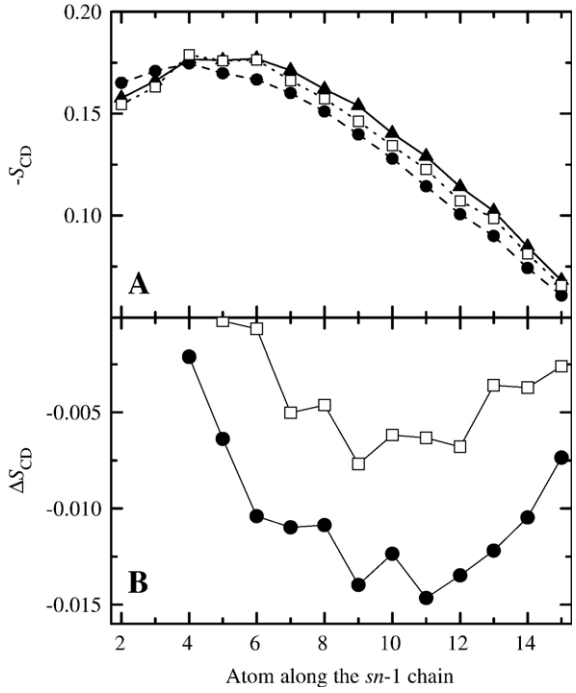

Fig. 5. (A) Deuterium order parameter S_{CD} of DPPC *sn*-1 chains calculated for DPPC (▲), 4 C6-NBD-PC:60 DPPC (●) and 4 C12-NBD-PC:60 DPPC (□) bilayers. (B) Difference between S_{CD} of DPPC *sn*-1 chains calculated for DPPC and those obtained for 4 C6-NBD-PC:60 DPPC (●) and 4 C12-NBD-PC:60 DPPC (□) bilayers, highlighting the decrease in acyl chain order parameter in the presence of the probes, most notably in the C9–C12 region.

(based on the coordinates of atoms $i-1$ and $i+1$), we were unable to confirm this particular result.

This property of the NBD-PC probes is at variance with the reported effect of DPH [9], free pyrene [10] or pyrene-labeled PC [11]. For both the DPH and pyrene fluorophores, their rigid structures and preferential orientations along the bilayer normal result in an ordering effect.

Another important question concerning the effect of the probes on the host bilayer structure is the range of the induced perturbations [9–11]. To this purpose, we also evaluated deuterium order parameters for DPPC acyl chains located at varying distances from NBD-PC probes. For each simulation frame, we calculated the order parameter of all individual DPPC acyl chains from their coordinates, and we calculated the distance (denoted here by R) of each chain to the center of mass of the closest NBD-PC molecule. In this way, we were able to calculate average order parameters for DPPC molecules in the immediate vicinity of NBD-PC probes ($R<0.6$ nm), at intermediate distances (0.6 nm$<R<$1.2 nm) and at larger distances ($R>1.2$ nm) to the closest probe molecule. Results are shown in Fig. 6 for the two 4 NBD-PC:60 NBD-PC systems. It is clear that, whereas disordering effects are detectable even for DPPC molecules with no immediate NBD-PC neighbors, the most significant perturbations occur in molecules in close contact with probes. This is especially true for C6-NBD-PC (Fig. 6A). Because the labeled *sn*-2 chain of this probe does not extend nearly so much across the bilayer as that of C12-NBD-PC (see e.g. Fig. 8 of [21]), the disordering effect of the former is mostly concentrated in its immediate vicinity, whereas the large extension of the C12-NBD-PC *sn*-2 chain allows for a more uniform distribution of the perturbation among additional layers of neighbors.

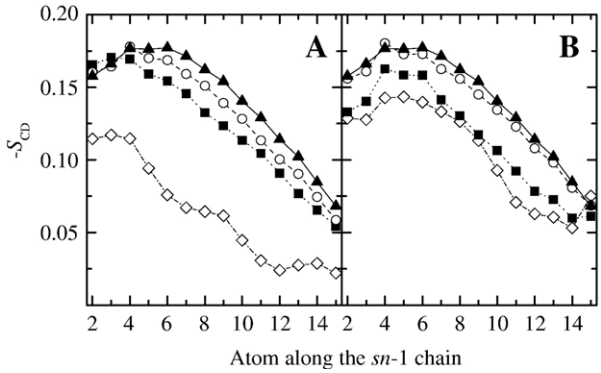

Fig. 6. Deuterium order parameter S_{CD} of DPPC *sn*-1 chains for different ranges of the distance R to the closest NBD-PC molecule in 4 C6-NBD-PC:60 DPPC (A) or 4 C12-NBD-PC:60 DPPC (B). Curves relative to $R<0.6$ nm (◇), 0.6 nm$<R<$1.2 nm (■), and $R>1.2$ nm (○) are shown, together with that obtained for pure, unperturbed DPPC (▲).

3.2.3. Mass density profiles

Because we previously discussed in detail the location and density profile of the NBD group [21], this section is focused on the effect of NBD-PC labeling on the water and lipid mass profiles and the bilayer thickness. A recent MD study of the effect of DPH on fluid DPPC reported an increase in bilayer thickness consistent with the ordering effect of the probe on the lipid acyl chains [9]. Taking into consideration that the effect of the NBD-PC probes on the chain order is opposite as discussed above, a decrease in bilayer thickness could be anticipated. However, as shown in Fig. 7, the incorporation of 4:60 probe: lipid ratio of both C6-NBD-PC and C12-NBD-PC does not alter significantly the mass density profiles of both water and total lipid (similar results were obtained for the 1:63 probe:lipid systems; not shown). Therefore, the bilayer thickness (operationally defined as the difference between the two transverse distance z values where local mass densities of water and lipid

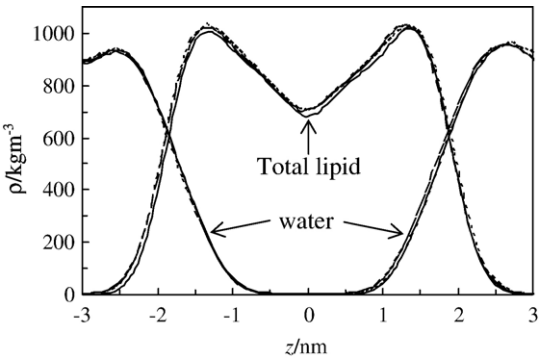

Fig. 7. Mass density profiles of water and total lipid as a function of transverse position relative to the center of the bilayer (z) obtained in the simulations of pure DPPC (solid lines), 4 C6-NBD-PC (dashed lines) and 4 C12-NBD-PC (dotted lines).

are equal) is not affected (the values obtained for the DPPC, 4 C6-NBD-PC:60 DPPC and 4 C12-NBD-PC:60 DPPC are all within 0.05 nm of each other, with an average of 3.75 nm). This somewhat intriguing result can be rationalized as the balance of two effects. On the one hand, on very close inspection, it can be seen that water penetration in the bilayer occurs to a slightly less extent in pure DPPC than in the probe-containing systems. This may be related to the expected effects as discussed above, and/or the result of efficient H-bonding involving water and the NBD fluorophore in labeled bilayers [21], and would per se imply a decrease in bilayer thickness. On the other hand, being the NBD-PC *sn*-2 chains heavier than those of DPPC, the lipid mass density profiles, even in the absence of a specific effect, would be very slightly broader in absolute terms than those of pure DPPC. This is compounded by the fact that the mass increase due to the fluorophore group occurs mainly near the water/lipid interface, and would lead per se to an *increase* in bilayer width as defined above. Both effects are very minor, and probably cancel each other, leading to an overall absence of significant influence of NBD-PC probes on the bilayer width.

3.2.4. Electrostatic potential

Given the polarity of the NBD fluorophore, it can be expected beforehand that incorporation of NBD-PC in the bilayer affects the electrostatic profile. Fig. 8 compares the profiles obtained for the DPPC, 4 C6-NBD-PC:60 DPPC and 4 C12-NBD-PC:60 DPPC systems. The value for pure DPPC, −0.55 V, agrees with recent MD studies [9,46] and lies within the range of experimental values [47–50]. Fig. 8A shows that both NBD-PC probes increase the difference in electrostatic potential between the interior of the bilayer and the bulk water phase. The values −0.58 V and −0.64 V were calculated for 4 C6-NBD-PC:60 DPPC and 4 C12-NBD-PC:60 DPPC, respectively. Whereas these values are subject to uncertainty due to cancellation errors because the observed potential profile is the difference between the water and lipid contributions, which almost cancel each other (see Fig. 8B), there is no doubt regarding the qualitative effect of the NBD-probe. This is most clearly seen in the (admittedly unphysical) splitting of the contributions to the electrostatic potential caused by the different types of molecules, shown in Fig. 8B for 4 C6-NBD-PC:60 DPPC (the same effect is verified for C12-NBD-PC, with minor quantitative differences; not shown). In the figure, the contribution of the C6-NBD-PC molecules was multiplied by the DPPC:NBD-PC mole ratio (15) to allow a direct comparison to that of DPPC. As shown in the figure, replacement of DPPC with C6-NBD-PC results in a less negative contribution to the overall potential that, when added to the water component, results in a larger potential across the membrane. A possible origin for this effect is that the snorkeling of the NBD group leads to the appearance of a strong dipole with the negative end (the oxygen atoms of the NO_2 group, O50–O51 in Fig. 1) oriented towards the water phase [21], opposing the choline–phosphate charge separation of the headgroups. Alternatively, the decreased membrane potential in the presence of NBD-PC may be related to the increased area per lipid molecule, following the experimental relationship verified by Clarke [51] for a series of PCs.

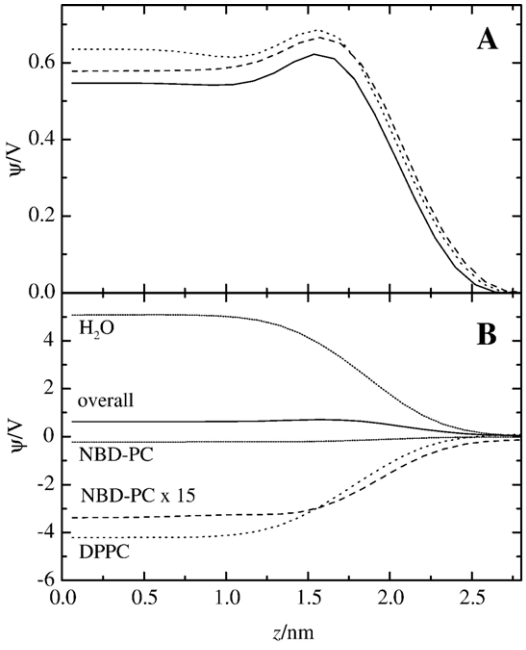

Fig. 8. (A) Electrostatic potential profiles for DPPC (solid line), 4 C6-NBD-PC:60 DPPC (dashed line) and 4 C12-NBD-PC:60 DPPC (dotted line) systems. (B) Splitting of molecular contributions to the overall electrostatic potential profile of 4 C6-NBD-PC:60 DPPC. The contribution of the C6-NBD-PC molecules was also multiplied by the DPPC:NBD-PC mole ratio (15) to allow a direct comparison to that of DPPC.

3.2.5. Effects on the water/lipid interface

The potential perturbation effects caused by NBD-PC probes on the interface region of the bilayer were studied by monitoring two interface parameters, the orientation of water relative to the bilayer normal (cosine of the angle between the latter and the water dipole moment) and the distribution of the angle between the P–N DPPC vector and the bilayer normal. In both cases, only minimal variations were found. Small changes in water order were observed, which correlated to the small variations in bilayer thickness discussed above, without any significant change in the shape of the orientation profile (not shown). On the other hand, the probability density function of the tilt angle of the P–N vector of the DPPC headgroups relative to the bilayer normal is virtually unaffected by the presence of NBD-PC. Broad, virtually indistinguishable distributions are recovered in all cases (not shown), with averages of 78.1° for pure DPPC (in excellent agreement with the value of 78.2° obtained by Repáková et al. [9]), 78.2° for both 1 NBD-PC:63 DPPC systems and 77.7° for both 4 NBD-PC:60 DPPC systems.

Both sets of results indicate that the snorkeling of NBD does not induce major perturbations on the structure of the lipid/water interface, possibly due to the fact that, according to our own simulations [21], and in agreement with NMR measurements [20], the most probable location of the fluorophore is near the glycerol backbone/carbonyl atoms of DPPC, and not the headgroup region.

3.2.6. Effect of NBD-PC on the dynamics of DPPC

Besides potentially causing perturbation of the bilayer structure, fluorescent probes can also affect both rotational and

lateral translational diffusion of the host lipid molecules. In order to study the rotational properties of different parts of the DPPC molecule, rotational autocorrelation functions $C(t)$ were calculated, as defined below:

$$C(t) = \langle P_2(\cos\theta(\xi))\rangle \tag{3}$$

where $\theta(\xi)$, for the sake of commodity, is the angle between a vector defined in the molecular framework at times ξ and $t+\xi$, and $P_2(x)=(3x^2-1)/2$ is the second order Legendre polynomial. Averaging is performed over ξ, which assuming a sufficiently ergodic trajectory, is an approximation of the ensemble average. Three vectors of the DPPC molecules were selected for analysis: the P–N axis (atoms 4 and 8 in Fig. 1) and the vectors uniting the 2nd and 15th carbon atoms of both *sn*-1 (atoms 18 and 31 in Fig. 1) and *sn*-2 (atoms 36 and 49 in Fig. 1) acyl chains. In this way, motions both in the headgroup and the hydrophobic regions of the bilayer were addressed.

All calculated $C(t)$ functions decay to a residual value $C_\infty > 0$, probably denoting hindered rotation (see e.g. discussion in [21]). Similar values of $C_\infty = 0.035$–0.040 and 0.19–0.22 were verified for the P–N and acyl chains' motions (respectively) in all systems. For the purpose of comparing the rotational dynamics across the five runs, the autocorrelation curves were analyzed using a double-exponential decay function with offset

$$C(t) = C_0[\beta_1 \exp(-t/\phi_1) + \beta_2 \exp(-t/\phi_2)] + C_\infty \tag{4}$$

and average rotational correlation times were calculated (correcting for the residual limiting value) using

$$\text{Average rotational time} = \frac{\int_0^\infty t(C(t)-C_\infty)dt}{\int_0^\infty (C(t)-C_\infty)dt} = \frac{\sum_{i=1}^{2}\beta_i\phi_i^2}{\sum_{i=1}^{2}\beta_i\phi_i} \tag{5}$$

Table 1 shows the average rotation correlation times for rotation of the three molecular vectors in all systems. Looking at the P–N axis, it is clear that whereas C6-NBD-PC has little effect on its rotation dynamics, incorporation of C12-NBD-PC leads to significantly slower dynamics. This can also be seen in Fig. 9A, which shows the autocorrelation functions. Similar conclusions can be drawn regarding the acyl chains' rotational motions (see Table 1). The different behaviors of the two probes in this regard may be related to the fact that the NBD group has a slightly more external location in C12-NBD-PC than in C6-NBD-PC, as verified experimentally in POPC bilayers [20] and as expected from our own simulations in fluid DPPC [21]. Therefore, the NBD group will be more likely to protrude into the headgroup region in C12-NBD-PC labeled bilayers, hindering to some extent the rotation of the host lipids. On the other hand, because of its longer, overstretched *sn*-2 chain (see Fig. 8 of [21]), C12-NBD-PC molecules probably act as obstacles to motions of neighboring acyl chains.

Table 1
Dynamic parameters of DPPC in absence and presence of NBD-PC

System	Average rotational correlation time/ns			$D/10^{-8}$ cm^2 s^{-1}
	P–N axis	*sn*-1 long axis	*sn*-2 long axis	
DPPC	1.3±0.1	1.5±0.2	1.5±0.2	9.9±2.4
1 C6-NBD-PC:63 DPPC	1.1±0.1	1.0±0.1	1.1±0.1	5.5±3.1
1 C12-NBD-PC:63 DPPC	2.0±0.2	2.5±0.3	2.7±0.4	9.4±0.7
4 C6-NBD-PC:60 DPPC	1.4±0.1	1.6±0.1	1.2±0.1	7.8±5.9
4 C12-NBD-PC:60 DPPC	3.9±0.3	2.7±0.3	2.6±0.3	6.5±3.8

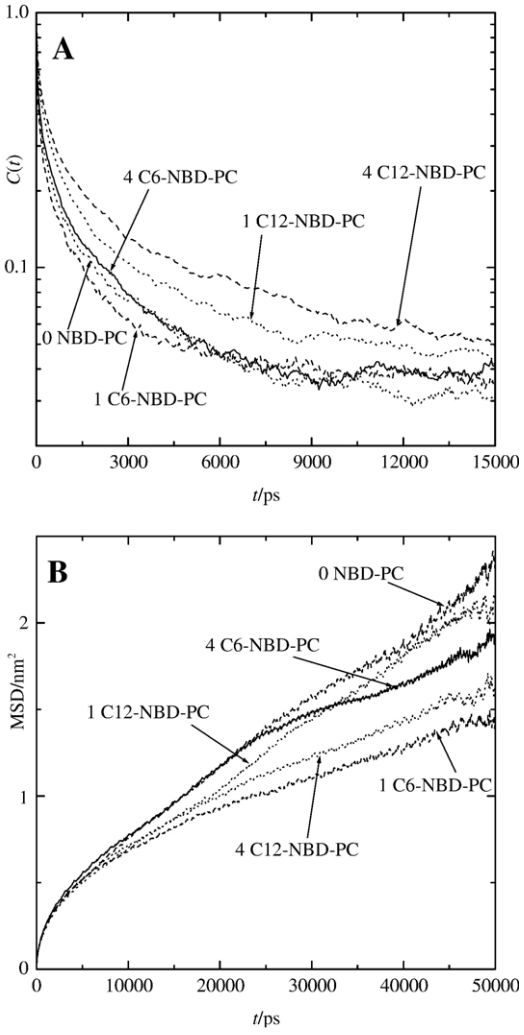

Fig. 9. (A) Autocorrelation functions $C(t)$ of the DPPC P–axis and (B) mean square displacement MSD(t) of DPPC molecules for all studied systems.

Lateral diffusion coefficients of the DPPC in all systems were calculated from the two-dimensional mean square displacement (MSD), using the Einstein relation

$$D = \frac{1}{4}\lim_{t\to\infty}\frac{d\text{MSD}(t)}{dt} \tag{6}$$

In turn, MSD is defined by

$$\mathrm{MSD}(t) = \langle || \vec{r_i}(t+t_0) - \vec{r_i}(t_0) || \rangle^2 \quad (7)$$

where $\vec{r_i}$ is the (x, y) position of the center of mass of molecule i of a given species, the averaging is carried out over all molecules of this kind and time origins t_0. To eliminate noise due to fluctuations in the center of mass of each monolayer, all MSD analysis was carried out using trajectories with fixed center of mass of one of the monolayers [33,52], and the final result is averaged over the two monolayers.

Fig. 9B shows MSD(t) for all simulated systems, whereas the corresponding D values are given in Table 1. As commented elsewhere [21], the value for DPPC shows excellent agreement with published experimental results for this phospholipid above the main transition temperature, using techniques such as pulsed NMR [53], quasi-elastic neutron scattering [54] and a spin-label photobleaching method [55], as well as with published values from MD simulations [35,43,52]. In our analysis, a wide uncertainty interval was obtained for D in this particular system, implying that there is overlap between the interval of DPPC and each of the intervals obtained for the other systems. Bearing this in mind, from inspection of both the MSD profiles and the recovered D values, it seems that lateral diffusion of DPPC molecules is generally slower in the presence of probe molecules. For C12-NBD-PC, D decreases with increased probe content. This was not verified for C6-NBD-PC, possibly due to the worse statistics obtained in the 1 C6-NBD-PC:63 DPPC system (for which the linear correlation coefficient between MSD and t was smallest), where the recovered D value is suspiciously low.

An alternative approach to the study of the effect of probe incorporation on DPPC diffusion is to calculate the short-time displacements $\Delta|\vec{r}| = \langle|\vec{r}(t+dt) - \vec{r}(t)|\rangle$, where $\vec{r}(t)$ is the position of the center of mass of a given DPPC at time t, and the brackets indicate averaging over time and DPPC molecules. Fig. 10 shows the calculated $\Delta|\vec{r}|$ with dt=200 ps for the various systems. The average displacements obtained for all probe-containing systems are lower than for pure DPPC. Although the differences are of the order of magnitude of the estimated errors, there seems to be a significant effect, as there is no overlap between the uncertainty intervals of DPPC and each of the probe-containing systems, with the sole exception of C12-NBD-PC (partly due to the larger error estimated for this system). On the other hand, from this study, the effect of replacing four DPPC molecules instead of a single one is possibly not significant.

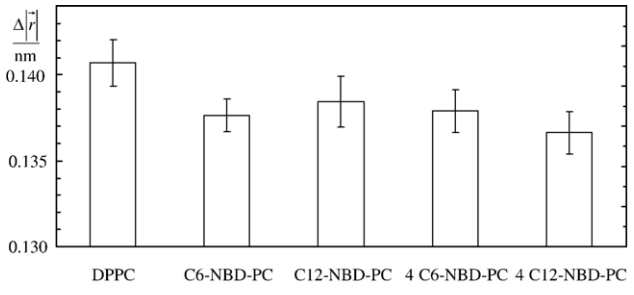

Fig. 10. $\Delta|\vec{r}| = \langle|\vec{r}(t+dt) - \vec{r}(t)|\rangle$ for all studied systems (dt=200 ps; see text for additional details).

In any case, even if the results are not totally conclusive, they suggest that lateral diffusion of DPPC is slower in bilayers containing NBD-PC (and C12-NBD-PC in particular) than in pure phospholipid, similarly to the rotational diffusion of the acyl chains discussed above. In a simplified depiction, this slower dynamics of DPPC in the presence of these probes could arise from the above mentioned overstretched conformation of the *sn*-2 chain of NBD-PC due to the snorkeling of the fluorophore, especially for the longer chain derivative (see Fig. 8 of [21]). In this scenario, the hinged *sn*-2 chains of NBD-PC could act as obstacles to diffusion of neighboring DPPC molecules.

3.2.7. Aggregation of NBD-PC in fluid DPPC bilayers

In principle, atomistic MD simulations can naturally report on nonhomogeneous distribution of membrane components. However, limitations in the time range and size of the simulated system, and (in this study in particular) the number of probe molecules (two in each leaflet in the 4 NBD-PC runs) do not allow for a definite study of probe-enriched domain formation. In any case, we investigated the possibility of NBD dimer formation by calculating the fraction of time (analyzing in the [20 ns, 100 ns] time range) that probe molecules are laterally separated by <0.8 nm in the 4 NBD-PC runs. The main conclusions (detailed results not shown) are the following:

(i) Complexes involving fluorophores located in opposing leaflets are most probably not significant (taking up, on average, 6% of the analyzed time range, and no more than 12% for any individual pair).
(ii) Complexes involving fluorophores located in the same leaflet were not observed for 4 C12-NBD-PC (taking up, on average, 5% of the analyzed time range, and no more than 7% for any individual pair).
(iii) However, NBD fluorophores of C6-NBD-PC located in the same leaflet are within 0.8 nm of each other for a significant amount of time. Two such "complexes" were observed, one in each leaflet, taking up ~40% of the analyzed time in both cases.

This latter observation could possibly be related to the fluorescence self-quenching displayed by these probes. It is, however, intriguing that no dimers were observed in C12-NBD-PC. Additional work is required to confirm this effect, both theoretical and experimental (fluorescence quenching and resonance energy transfer studies).

4. Concluding remarks

Following our recent work on the location and dynamics of NBD-PC probes incorporated in fluid DPPC bilayers [21], this study focused on the potential effects of these molecules in the host bilayer, from both theoretical (MD simulations) and experimental (DSC scans) points of view. From the MD simulations, it is concluded that, whereas a number of parameters (e.g. area/lipid, lipid chain order parameters) are not severely affected for 1:63 probe:DPPC ratio (1.6 mol%), for the higher concentration studied (4:60 probe:DPPC ratio, 6.2 mol%) important differences are evident. In agreement with experimental

observations by other authors, the average area per phospholipid molecule increases, whereas DPPC acyl chain order parameters decrease, most importantly in the C9–C12 region. Incorporation of NBD-PC molecules also increases the electrostatic potential across the bilayer, and, especially for the long *sn*-2 chain derivative, apparently slows the lateral diffusion of DPPC molecules and the rotational mobility of DPPC acyl chains.

Of course, being fluorescence spectroscopy a very sensitive technique (and given that the NBD fluorophore has good values of absorption coefficient and emission quantum yield in membranes), in a carefully designed experiment, there should be no need to use high (>5 mol%) probe concentrations, and, for most cases (depending on the quality of fluorescence instrumentation available), 0.1–0.5 mol% will suffice. Due to computational limitations, we were not able to study systems containing these lower probe concentrations (which would necessarily imply very large simulated bilayers), but, judging from the 1 NBD-PC:63 DPPC simulations, severe structural and dynamical perturbations of fluid bilayers are not expected.

However, this is no longer the case regarding the thermotropic behavior of DPPC. Our DSC study revealed that even small amounts (<1 mol%) of NBD-PC lead to the elimination of the pre-transition and to a large loss of cooperativity of the main transition of DPPC. Interestingly, shifts of T_m in opposite directions were observed for the two studied probes. Throughout the MD simulations analyses, similar patterns were observed for the effects of C6-NBD-PC and C12-NBD-PC. Minor differences (mainly in the effect on DPPC rotational and translational mobility) could be attributed to the slightly more external location of the NBD moiety in C12-NBD-PC, as well as to its longer, stretched *sn*-2 chain ([20,21]). However, the DSC scans of C6-NBD-PC and C12-NBD-PC-containing DPPC vesicles are markedly different, and the fact that T_m decreases upon incorporation of C6-NBD-PC but increases upon incorporation of C12-NBD-PC could not be related to our simulation results in fluid DPPC. In truth, this should not be surprising, as the main transition of DPPC also involves the gel phase, for which no MD simulations were carried out. In case that the two probes affect differently the structure of the considerably more rigid gel phase, it is expected that they will cause qualitatively different alterations in the thermotropic behavior of DPPC. In particular, the higher values of transition temperature and enthalpy of DPPC/C12-NBD-PC samples relative to pure DPPC point to increased magnitude of mixed DPPC/probe interactions (relative to DPPC/DPPC interactions) in the gel phase. Recently, from fluorescence measurements (red-edge excitation shift spectroscopy) it was suggested that snorkeling of the NBD group of NBD-PC may not occur in gel phase DPPC [56]. We are currently testing this interesting hypothesis using MD simulations. On the other hand, being the probe molecules themselves phospholipids (with an intact *sn*-1 chain and a modified *sn*-2 chain), they obviously contribute directly to the thermotropic behavior of the system. It is well known that longer chain phospholipids undergo main transition at higher temperatures and with higher transition enthalpy [57]. In this view, it is not surprising that C12-NBD-PC-containing vesicles will have higher T_m and transition enthalpy than C6-NBD-PC-containing vesicles. What is more interesting is that i) the T_m for pure DPPC falls in between the T_m values observed for C6-NBD-PC and C12-NBD-PC-labeled DPPC vesicles, and ii) a very considerable broadening of the transition is evident even for very low probe concentration. The origin of such a large loss in transition cooperativity is not clear from our simulations, and is possibly related to probe-induced perturbation of the DPPC gel matrix. This correlates with the appearance of two peaks in the scans of the samples with highest probe content, denoting phase separation into two kinds of domains below T_m, which would melt at slightly different temperatures. In any case, it severely hampers the use of these probes in the monitorization of PC thermotropic transitions. For this purpose, a suitable alternative is provided by DPH, for which concentrations in excess of 2 mol% in DPPC vesicles change T_m by less than 0.1 °C, do not suppress either the pre-transition or the subtransition, and leave the peak width (and hence the transition cooperativity) of the main transition unaltered [9].

Finally, our study (together with other recent works; [9–11, 35]) reinforces the usefulness of MD simulations (especially when used in conjunction with experimental techniques) as a tool to predict the effect of fluorescent membrane probes on the host bilayer structure, in order to select suitable probes and conditions for minimal membrane perturbation.

Acknowledgements

Financial support for this work was provided by FCT (Portugal) through projects PPCDT/SAU-FCF/56003/2004 and PPCDT/QUIM/57114/2004. F. F. acknowledges grant SFRH/BD/14282/2003 from FCT (Portugal).

References

[1] J.R. Silvius, I.R. Nabi, Fluorescence-quenching and resonance energy transfer studies of lipid microdomains in model and biological membranes, Mol. Membr. Biol. 23 (2006) 5–16.
[2] L. Bagatolli, To see or not to see: lateral organization of biological membranes and fluorescence microscopy, Biochim. Biophys. Acta 1758 (2006) 1541–1556.
[3] W. Lesslauer, J.E. Cain, J.K. Blasie, X-Ray diffraction studies of lecithin bimolecular leaflets with incorporated fluorescent probes, Proc. Natl. Acad. Sci. U. S. A. 69 (1972) 1499–1503.
[4] D.A. Cadenhead, B.M.J. Kellner, K. Jacobson, D. Papahadjopoulos, Fluorescent probes in model membranes I: anthroyl fatty acid derivatives in monolayers and liposomes of dipalmitoylphosphatidylcholine, Biochemistry 16 (1977) 5386–5392.
[5] R.D. Klausner, D.E. Wolf, Selectivity of fluorescent lipid analogues for lipid domains,, Biochemistry 19 (1980) 6199–6203.
[6] R.G. Ashcroft, K.R. Thulborn, J.R. Smith, H.G.L. Coster, W.H. Sawyer, Perturbations to lipid bilayers by spectroscopic probes as determined by dielectric measurements, Biochim. Biophys. Acta 602 (1980) 299–308.
[7] W.L. Ash, M.R. Zlomislic, E.O. Oloo, D.P. Tieleman, Computer simulations of membrane proteins, Biochim. Biophys. Acta 1666 (2004) 158–189.
[8] H.L. Scott, Modeling the lipid component of membranes, Curr. Opin. Struct. Biol. 12 (2002) 495–502.
[9] J. Repáková, J.M. Holopainen, M.R. Morrow, M.C. McDonald, P. Čapková, I. Vattulainen, Influence of DPH on the structure and dynamics of a DPPC bilayer, Biophys. J. 88 (2005) 3398–3410.
[10] J. Čurdová, P. Čapková, J. Plášek, J. Repáková, I. Vattulainen, Free pyrene probes in gel and fluid membranes: perspective through atomistic simulations, J. Phys. Chem., B 111 (2007) 3640–3650.
[11] J. Repáková, J.M. Holopainen, M. Karttunen, I. Vattulainen, Influence of pyrene-labeling on fluid lipid membranes, J. Phys. Chem. B 110 (2006) 15403–15410.

[12] A. Chattopadhyay, Chemistry and biology of *N*-(7-nitrobenz-2-oxa-1, 3-diazol-4-yl)-labeled lipids — fluorescent-probes of biological and model membranes, Chem. Phys. Lipids 53 (1990) 1–15.
[13] S. Mazères, V. Schram, J.F. Tocanne, A. Lopez, A, 7-nitrobenz-2-oxa-1, 3-diazole-4-yl-labeled phospholipids in lipid membranes: differences in fluorescence behaviour, Biophys. J. 71 (1996) 327–335.
[14] S. Mukherjee, H. Raghuraman, S. Dasgupta, A. Chattopadhyay, Organization and dynamics of *N*-(7-nitrobenz-2-oxa-1,3-diazol-4-yl)-labeled lipids: a fluorescence approach, Chem. Phys. Lipids 127 (2004) 91–101.
[15] U. Marx, G. Lassmann, H.G. Holzhütter, D. Wüstner, P. Müller, A. Höhlig, J. Kubelt, A. Herrmann, Rapid flip-flop of phospholipids in endoplasmic reticulum membranes studied by a stopped-flow approach, Biophys. J. 78 (2000) 2628–2640.
[16] C. Leidy, W.F. Wolkers, K. Jørgensen, O.G. Mouritsen, J.H. Crowe, Lateral organization and domain formation in a two-component lipid membrane system, Biophys. J. 80 (2001) 1819–1828.
[17] L.M.S. Loura, A. Coutinho, A. Silva, A. Fedorov, M. Prieto, Structural effects of a basic peptide on the organization of dipalmitoylphosphatidylcholine/dipalmitoylphosphatidylserine membranes: a fluorescent resonance energy transfer study, J. Phys. Chem., B 110 (2006) 8130–8141.
[18] F.S. Abrams, E. London, Extension of the parallax analysis of membrane penetration depth to the polar-region of model membranes — use of fluorescence quenching by a spin-label attached to the phospholipid polar headgroup, Biochemistry 32 (1993) 10826–10831.
[19] A. Chattopadhyay, E. London, Parallax method for direct measurement of membrane penetration depth utilizing fluorescence quenching by spin-labeled phospholipids, Biochemistry 26 (1987) 39–45.
[20] D. Huster, P. Müller, K. Arnold, A. Herrmann, Dynamics of membrane penetration of the fluorescent 7-nitrobenz-2-oxa-1,3-diazol-4-yl (NBD) group attached to an acyl chain of phosphatidylcholine, Biophys. J. 80 (2001) 822–831.
[21] L.M.S. Loura, J.P.P. Ramalho, Location and dynamics of acyl chain NBD-labeled phosphatidylcholine (NBD-PC) in DPPC bilayers. A molecular dynamics and time-resolved fluorescence anisotropy study, Biochim. Biophys. Acta 1768 (2007) 467–478.
[22] R.P. Haugland, Handbook of Fluorescent Probes and Research Chemicals, 6th ed. Molecular Probes, Eugene, OR, 1996.
[23] C.W.F. McClare, An accurate and convenient organic phosphorus assay, Anal. Biochem. 39 (1971) 527–530.
[24] M.P. Veiga, J.L. Arrondo, F.M. Goñi, A. Alonso, Ceramides in phospholipid membranes: effects on bilayer stability and transition to non-lamellar phases, Biophys. J. 76 (1999) 342–350.
[25] H.J.C. Berendsen, J.P.M. Postma, W.F. van Gunsteren, J. Hermans, Interaction models for water in relation to protein hydration, in: B. Pullman (Ed.), Intermolecular Forces, Reidel, Dordrecht, The Netherlands, 1981, pp. 331–342.
[26] J.F. Nagle, R. Zhang, S. Tristram-Nagle, W. Sun, H.I. Petrache, R.M. Suter, X-ray structure determination of fully hydrated L alpha phase dipalmitoylphosphatidylcholine bilayers, Biophys. J. 70 (1996) 1419–1431.
[27] H.J.C. Berendsen, D. van der Spoel, R. van Drunen, GROMACS: a message-passing parallel molecular dynamics implementation, Comp. Phys. Comm. 91 (1995) 43–56.
[28] E. Lindahl, B. Hess, D. van der Spoel, GROMACS 3.0: a package for molecular simulation and trajectory analysis, J. Mol. Model 7 (2001) 306–317.
[29] H.J.C. Berendsen, J.P.M. Postma, A. DiNola, J.R. Haak, Molecular dynamics with coupling to an external bath, J. Chem. Phys. 81 (1984) 3684–3690.
[30] S. Miyamoto, P.A. Kollman, SETTLE: an analytical version of the SHAKE and RATTLE algorithms for rigid water models, J. Comput. Chem. 13 (1992) 952–962.
[31] B. Hess, H. Bekker, H.J.C. Berendsen, J.G.E.M. Fraaije, LINCS: a linear constraint solver for molecular simulations, J. Comput. Chem. 18 (1997) 1463–1472.
[32] K.A. Feenstra, B. Hess, H.J.C. Berendsen, Improving efficiency of large time-scale molecular dynamics simulations of hydrogen-rich systems, J. Comput. Chem. 20 (1999) 786–798.
[33] C. Anézo, C.A.H. de Vries, H.-D. Höltje, D.P. Tieleman, S.-J. Marrink, Methodological issues in lipid bilayer simulations, J. Phys. Chem., B 107 (2003) 9424–9433.
[34] U. Essman, L. Perela, M.L. Berkowitz, T. Darden, H. Lee, L.G. Pedersen, A smooth particle mesh Ewald method, J. Chem. Phys. 103 (1995) 8577–8592.
[35] J. Repáková, P. Čapková, J.M. Holopainen, I. Vattulainen, Distribution orientation and dynamics of DPH probes in DPPC bilayer, J. Phys. Chem., B 108 (2004) 13438–13448.
[36] O. Berger, O. Edholm, F. Jahnig, Molecular dynamics simulations of a fluid bilayer of dipalmitoylphosphatidylcholine at full hydration constant, pressure, and constant temperature, Biophys. J. 72 (1997) 2002–2013.
[37] D.P. Tieleman, H.J.C. Berendsen, Molecular dynamics simulations of a fully hydrated dipalmitoyl phosphatidylcholine bilayer with different macroscopic boundary conditions and parameters, J. Chem. Phys. 105 (1996) 4871–4880.
[38] S. Mabrey, J.M. Sturtevant, Investigation of phase transitions of lipids and lipid mixtures by high sensitivity differential scanning calorimetry, Proc. Natl. Acad. Sci. U. S. A. 73 (1976) 3862–3866.
[39] N. Fang, V. Chan, H.-Q. Mao, K.W. Leong, Interactions of phospholipid bilayer with chitosan: effect of molecular weight and pH, Biomacromolecules 2 (2001) 1161–1168.
[40] H.-J. Hinz, J.M. Sturtevant, Calorimetric studies of dilute aqueous suspensions of bilayers formed from synthetic L-α-lecithins, J. Biol. Chem. 247 (1972) 6071–6075.
[41] E. Falck, M. Patra, M. Karttunen, M.T. Hyvönen, I. Vattulainen, Lessons of slicing membranes: interplay of packing, free area, and lateral diffusion in phospholipid/cholesterol bilayers, Biophys. J. 87 (2004) 1076–1091.
[42] S.W. Chiu, E. Jacobsson, R.J. Mashl, H.L. Scott, Cholesterol-induced modifications in lipid bilayers: a simulation study, Biophys. J. 83 (2002) 1842–1853.
[43] C. Hofsäß, E. Lindahl, O. Edholm, Molecular dynamics simulations of phospholipid bilayers with cholesterol, Biophys. J. 84 (2003) 2192–2206.
[44] R.B. Gennis, Biomembranes: Molecular Structure and Function, Springer-Verlag, New York, 1989.
[45] D.P. Tieleman, S.J. Marrink, H.J.C. Berendsen, A computer perspective of membranes: molecular dynamics studies of lipid bilayer systems, Biochim. Biophys. Acta 1331 (1997) 235–270.
[46] M. Patra, M. Karttunen, M.T. Hyvönen, E. Falck, P. Lindqvist, I. Vattulainen, Molecular dynamics simulations of lipid bilayers: major artifacts due to truncating electrostatic interactions, Biophys. J. 84 (2003) 3636–3645.
[47] R.F. Flewelling, W.L. Hubbell, The membrane dipole potential in a total membrane potential model, Biophys. J. 49 (1986) 541–552.
[48] S.A. Simon, T.J. McIntosh, Magnitude of the solvation pressure depends on dipole potential, Proc. Natl. Acad. Sci. U. S. A. 86 (1989) 9263–9267.
[49] K. Gawrisch, D. Ruston, J. Zimmerberg, V.A. Parsegian, R.P. Rand, N. Fuller, Membrane dipole potentials hydration forces, and the ordering of water at membrane surface, Biophys. J. 61 (1992) 1213–1223.
[50] T.J. McIntosh, S.A. Simon, D. Needham, C.-H. Huang, Interbilayer interactions between sphingomyelin and sphingomyelin/cholesterol bilayers, Biochemistry 31 (1992) 2020–2024.
[51] R.J. Clarke, Effect of lipid structure on the dipole potential of phosphatidylcholine bilayers, Biochim. Biophys. Acta 1327 (1997) 269–278.
[52] E. Lindahl, O. Edholm, Molecular dynamics simulation of NMR relaxation rates and slow dynamics in lipid bilayers, J. Chem. Phys. 115 (2001) 4938–4950.
[53] A.L. Kuo, C.G. Wade, Lipid lateral diffusion by pulsed nuclear magnetic-resonance, Biochemistry 18 (1979) 2300–2308.
[54] S. König, W. Pfeiffer, T. Bayerl, D. Richter, E. Sackmann, Molecular-dynamics of lipid bilayers studied by incoherent quasi-elastic neutron-scattering, J. Phys., II 2 (1992) 1589–1615.
[55] J.R. Sheats, H.M. McConnell, Photo-chemical technique for measuring lateral diffusion of spin-labeled phospholipids in membranes, Proc. Natl. Acad. Sci. U. S. A. 75 (1978) 4661–4663.
[56] T.J. Pucadyil, S. Mukherjee, A. Chattopadhyay, Organization and dynamics of NBD-labeled lipids in membranes analyzed by fluorescence recovery after photobleaching, J. Phys. Chem. B 111 (2007) 1975–1983.
[57] G. Cevc, D. Marsh, Phospholipid Bilayers: Physical Principles and Models, Wiley, Chichester, UK, 1987.